



**AFRL-RX-WP-JA-2017-0191**

**MICROSTRUCTURE EVOLUTION AND MECHANICAL  
BEHAVIOR OF ULTRAFINE Ti6Al4V DURING  
LOW-TEMPERATURE SUPERPLASTIC  
DEFORMATION (POSTPRINT)**

**S.L Semiatin  
AFRL/RX**

**S.V. Zharebtsov, E.A. Kudryavtsev, and G.A. Salishchev  
Belgorod State University**

**B.B. Straumal  
Russian Academy of Science**

**23 June 2016  
Interim Report**

**Distribution Statement A.  
Approved for public release: distribution unlimited.**

**© 2016 ELSEVIER LTD**

**(STINFO COPY)**

**AIR FORCE RESEARCH LABORATORY  
MATERIALS AND MANUFACTURING DIRECTORATE  
WRIGHT-PATTERSON AIR FORCE BASE, OH 45433-7750  
AIR FORCE MATERIEL COMMAND  
UNITED STATES AIR FORCE**

<b>REPORT DOCUMENTATION PAGE</b>				<i>Form Approved</i> OMB No. 0704-0188	
The public reporting burden for this collection of information is estimated to average 1 hour per response, including the time for reviewing instructions, searching existing data sources, gathering and maintaining the data needed, and completing and reviewing the collection of information. Send comments regarding this burden estimate or any other aspect of this collection of information, including suggestions for reducing this burden, to Department of Defense, Washington Headquarters Services, Directorate for Information Operations and Reports (0704-0188), 1215 Jefferson Davis Highway, Suite 1204, Arlington, VA 22202-4302. Respondents should be aware that notwithstanding any other provision of law, no person shall be subject to any penalty for failing to comply with a collection of information if it does not display a currently valid OMB control number. <b>PLEASE DO NOT RETURN YOUR FORM TO THE ABOVE ADDRESS.</b>					
<b>1. REPORT DATE (DD-MM-YY)</b> 23 June 2016		<b>2. REPORT TYPE</b> Interim		<b>3. DATES COVERED (From - To)</b> 19 March 2014 – 23 May 2016	
<b>4. TITLE AND SUBTITLE</b> MICROSTRUCTURE EVOLUTION AND MECHANICAL BEHAVIOR OF ULTRAFINE Ti6Al4V DURING LOW-TEMPERATURE SUPERPLASTIC DEFORMATION (POSTPRINT)				<b>5a. CONTRACT NUMBER</b> IN-HOUSE	
				<b>5b. GRANT NUMBER</b>	
				<b>5c. PROGRAM ELEMENT NUMBER</b>	
<b>6. AUTHOR(S)</b> 1) S.L. Semiatin - AFRL/RX      2) S.V. Zharebtsov, E.A. Kudryavtsev, and G.A. Salishchev - Belgorod State University (Continued on pg. 2)				<b>5d. PROJECT NUMBER</b>	
				<b>5e. TASK NUMBER</b>	
				<b>5f. WORK UNIT NUMBER</b> X0W6	
<b>7. PERFORMING ORGANIZATION NAME(S) AND ADDRESS(ES)</b> 1) AFRL/RX Wright Patterson AFB, OH 45433      2) Belgorod State University 85 Pobeda Str., Belgorod 308015 Russia (Continued on pg. 2)				<b>8. PERFORMING ORGANIZATION REPORT NUMBER</b>	
<b>9. SPONSORING/MONITORING AGENCY NAME(S) AND ADDRESS(ES)</b> Air Force Research Laboratory Materials and Manufacturing Directorate Wright-Patterson Air Force Base, OH 45433-7750 Air Force Materiel Command United States Air Force				<b>10. SPONSORING/MONITORING AGENCY ACRONYM(S)</b> AFRL/RXCM	
				<b>11. SPONSORING/MONITORING AGENCY REPORT NUMBER(S)</b> AFRL-RX-WP-JA-2017-0191	
<b>12. DISTRIBUTION/AVAILABILITY STATEMENT</b> Distribution Statement A. Approved for public release: distribution unlimited.					
<b>13. SUPPLEMENTARY NOTES</b> PA Case Number: 88ABW-2016-3084; Clearance Date: 23 June 2016. This document contains color. Journal article published in Acta Materialia. © 2016 Elsevier Ltd. The U.S. Government is joint author of the work and has the right to use, modify, reproduce, release, perform, display, or disclose the work. The final publication is available at <a href="http://www.elsevier.com/locate/actamat">www.elsevier.com/locate/actamat</a> DOI: <a href="https://doi.org/10.1016/j.actamat.2016.09.003">https://doi.org/10.1016/j.actamat.2016.09.003</a>					
<b>14. ABSTRACT (Maximum 200 words)</b> The influence of microstructure evolution on the low-temperature superplasticity of ultrafine Ti6Al4V was established. For this purpose, the static and dynamic coarsening response and plastic-flow behavior of the alloy with a mean size of $\alpha$ (sub)grains and $\beta$ particles of 0.1–0.4 $\mu\text{m}$ were determined via a series of tension tests at temperatures between 450 and 700 °C. Both static and dynamic coarsening exhibited diffusion-controlled (r3-vs-time) kinetics. However, dynamic coarsening was approximately two orders of magnitude faster than the corresponding static behaviors due to enhanced diffusion through the deformed $\beta$ matrix. A total elongation of 1000% and strain-rate-sensitivity exponent $m = 0.48$ were obtained at 550 °C and $2 \times 10^{-4} \text{ s}^{-1}$ . Very limited cavitation was observed in the specimens after superplastic deformation under optimal conditions.					
<b>15. SUBJECT TERMS</b> Titanium alloy; Low-temperature superplasticity; Ultrafine structure; Microstructure coarsening					
<b>16. SECURITY CLASSIFICATION OF:</b>			<b>17. LIMITATION OF ABSTRACT:</b> SAR	<b>18. NUMBER OF PAGES</b> 15	<b>19a. NAME OF RESPONSIBLE PERSON (Monitor)</b> Bill Song <b>19b. TELEPHONE NUMBER (Include Area Code)</b> (937) 255-1351
<b>a. REPORT</b> Unclassified	<b>b. ABSTRACT</b> Unclassified	<b>c. THIS PAGE</b> Unclassified			

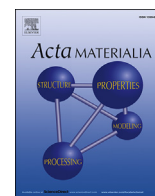
Standard Form 298 (Rev. 8-98)  
Prescribed by ANSI Std. Z39-18

**6. AUTHOR(S)**

3) B.B. Straumal - RAS

**7. PERFORMING ORGANIZATION NAME(S) AND ADDRESS(ES)**

3) Russian Academy of Sciences, Ac. Ossipyan Str. 2  
142432, Chernogolovka



## Full length article

# Microstructure evolution and mechanical behavior of ultrafine Ti–6Al–4V during low-temperature superplastic deformation

S.V. Zharebtsov <sup>a,\*</sup>, E.A. Kudryavtsev <sup>a</sup>, G.A. Salishchev <sup>a</sup>, B.B. Straumal <sup>b,c</sup>, S.L. Semiatin <sup>d</sup><sup>a</sup> Laboratory of Bulk Nanostructured Materials, Belgorod State University, 85 Pobeda Str., Belgorod, 308015, Russia<sup>b</sup> Institute of Solid State Physics, Russian Academy of Sciences, Ac. Ossipyan Str. 2, 142432, Chernogolovka, Russia<sup>c</sup> National University of Science and Technology «MISIS», Leninskii Pros. 4, 119049, Moscow, Russia<sup>d</sup> Air Force Research Laboratory, Materials and Manufacturing Directorate, AFRL/RXCM, Wright-Patterson AFB, OH, 45433-7817, USA

## ARTICLE INFO

## Article history:

Received 8 June 2016

Received in revised form

26 July 2016

Accepted 1 September 2016

Available online 13 September 2016

## Keywords:

Titanium alloy

Low-temperature superplasticity

Ultrafine structure

Microstructure coarsening

## ABSTRACT

The influence of microstructure evolution on the low-temperature superplasticity of ultrafine Ti–6Al–4V was established. For this purpose, the static and dynamic coarsening response and plastic-flow behavior of the alloy with a mean size of  $\alpha$  (sub)grains and  $\beta$  particles of 0.1–0.4  $\mu\text{m}$  were determined via a series of tension tests at temperatures between 450 and 700 °C. Both static and dynamic coarsening exhibited diffusion-controlled ( $r^3$ -vs-time) kinetics. However, dynamic coarsening was approximately two orders of magnitude faster than the corresponding static behaviors due to enhanced diffusion through the deformed  $\beta$  matrix. A total elongation of 1000% and strain-rate-sensitivity exponent  $m = 0.48$  were obtained at 550 °C and  $2 \times 10^{-4} \text{ s}^{-1}$ . Very limited cavitation was observed in the specimens after superplastic deformation under optimal conditions.

© 2016 Acta Materialia Inc. Published by Elsevier Ltd. All rights reserved.

## 1. Introduction

A considerable decrease in grain size to a range between 0.1 and 1  $\mu\text{m}$  can be attained through various techniques of severe or large plastic deformation. Such microstructure refinement leads to a noticeable improvement in some mechanical properties (e.g., monotonic and cyclic strength, hardness, wear resistance) as well as a significant reduction in the temperature for superplastic (SP) deformation. The latter benefit has attracted great interest due to the possibility to conduct superplastic forming (SPF) and/or SP-assisted diffusion bonding at temperatures much lower than those typically used for commercial production [e.g. 1, 2]. For example, Lutfullin, et al. [3] reported successful diffusion bonding of Ti–6Al–4V with an ultrafine microstructure ( $d = 0.2$ – $0.4 \mu\text{m}$ ) at the very low temperature of 600 °C. In addition, lower SPF temperatures can result in: (i) the retention of high service-temperature strength which is intrinsic to ultrafine-grain metals; (ii) reduced surface oxidation on SPF parts; (iii) the possibility of using less-expensive tool materials and (iv) decreased flow stress that considerably reduces tool wear during superplastic forming.

The decrease in SP deformation temperature associated with

microstructure refinement can be predicted from the Bird–Mukherjee–Dorn equation [4]:

$$\dot{\epsilon} = A \frac{DGb}{kT} \left( \frac{b}{d} \right)^p \left( \frac{\sigma}{G} \right)^n, \quad (1)$$

in which  $\dot{\epsilon}$  is the strain rate,  $kT$  is Boltzmann's constant times the absolute temperature,  $D$  is the dominant temperature-dependent diffusivity,  $G$  is the temperature-dependent shear modulus,  $b$  is Burgers vector,  $d$  is the grain size,  $n$  is the stress exponent ( $n = 1/m$ , where  $m$  is the strain-rate-sensitivity exponent); and  $p$  and  $A$  are constants. The low-temperature SP properties of two-phase titanium alloys with an ultrafine-grain microstructure developed via large deformation has been discussed in a number of earlier works [5–9]. For example, SP behavior was observed at 600 °C and a strain rate of  $5 \times 10^{-4} \text{ s}^{-1}$  in Ti–6Al–4V with a grain size of 0.3  $\mu\text{m}$  produced by warm multiaxial forging; the total elongation  $\delta$  and strain-rate-sensitivity coefficient  $m$  were 500% and 0.34, respectively [10]. The same alloy with the same grain size produced by ECAP showed  $\delta = 296\%$  and  $m = 0.34$  at 600 °C and  $1 \times 10^{-4} \text{ s}^{-1}$  [6].

The high-temperature SP behavior of various metallic materials, including titanium alloys, is usually the result of concurrent grain- or interphase-boundary sliding, grain-matrix dislocation activity, and diffusional creep [2]. However, the contribution of these

\* Corresponding author.

E-mail addresses: [ser\\_z@mail.ru](mailto:ser_z@mail.ru), [zharebtsov@bsu.edu.ru](mailto:zharebtsov@bsu.edu.ru) (S.V. Zharebtsov).

various mechanisms during SP flow of ultrafine-grain alloys may change with a reduction in temperature. For example, a decrease in the SP properties of two-phase titanium alloys may be expected due to a retardation in diffusion-controlled processes, an increase in the fraction of the  $\alpha$  phase (in which diffusion is much slower than that in the  $\beta$  phase [11]), and/or a decrease in the fraction of  $\beta$  per se. Another factor which may result in the decreased ductility is the propensity of ultrafine titanium alloys for grain/particle growth when the fraction of  $\beta$  phase decreases noticeably. Despite extensive investigations of the constitutive behavior during low temperature SP, detailed microstructure evolution data for ultrafine Ti–6Al–4V alloy have been presented only for temperatures above 775 °C [5].

The aim of the present work, therefore, was to quantify microstructure evolution and the mechanical behavior of warm-worked Ti–6Al–4V with 0.1–0.4  $\mu\text{m}$   $\alpha$  (sub)grains and  $\beta$  particles during SP deformation at the very low temperature of 550 °C. This investigation is particularly relevant for the industrial application of superplasticity due to the possibility of producing large-scale preforms with a sub(grain) or particle size of ~0.2–0.5  $\mu\text{m}$  by the large-plastic-deformation method of isothermal, multiaxial forging (MF). Furthermore, subsequent warm rolling of forgings with an ultrafine preform microstructure can yield commercial-size sheets with an average grain size of 0.65  $\mu\text{m}$ . A detailed description of these methods is given elsewhere [12–14].

## 2. Material and procedures

The program material consisted of the  $\alpha/\beta$  titanium alloy Ti–6Al–4V with a nominal composition (in weight pct.) of 6.3 Al, 4.1 V, 0.18 Fe, 0.03 Si, 0.02 Zr, 0.01 C, 0.18 O, 0.01 N. It was supplied in the form of a hot-rolled 40-mm diameter bar with a  $\beta$ -transus temperature of 990 °C. Bulk specimens measuring ~40 × 60 mm with an ultrafine microstructure were produced by MF under isothermal conditions. For this purpose, preforms which were water quenched following beta annealing at 1010 °C were worked in the temperature interval of 700 → 475 °C using a hydraulic press equipped with isothermal-forging tooling. The nominal strain rate was  $\sim 10^{-3} \text{ s}^{-1}$ . Following MF, 4-mm-thick rolling preforms were sectioned along the longitudinal axis by electric-discharge machining. To increase microstructure homogeneity and to form a specified (rolling) texture before SP tension testing, each plate was rolled to sheet at 475 °C under isothermal conditions. The reduction per pass was 5–10%. The total reduction was ~50%, thus yielding a final sheet thickness of 2 mm.

Dog-bone shaped tension specimens with a reduced section measuring  $12 \times 3 \times 1.5 \text{ mm}$  were machined from the sheets. Tension tests were performed in an Instron mechanical-testing machine at temperatures between 450 and 700 °C with a constant crosshead speed between 0.05 and 100 mm/min or a constant strain rate in the interval  $2 \times 10^{-5} \text{ s}^{-1}$ – $2 \times 10^{-3} \text{ s}^{-1}$  at 550 °C. The strain rate sensitivity  $m$  was evaluated using the slope of  $\log \sigma - \log \dot{\epsilon}$  curves or strain-rate-change tests [15]. Despite unavoidable, albeit typically small, variations in microstructure with temperature and strain rate, an *approximate* apparent activation energy for plastic deformation ( $Q$ ) was calculated from the semi-log dependence of the true flow stress  $\ln(\sigma/G)$  taken at a true strain  $\epsilon = 0.1$  on the inverse absolute temperature ( $1/T$ ) for  $\dot{\epsilon} = 5 \times 10^{-4} \text{ s}^{-1}$  and  $T = 450$ – $700$  °C.

The details of microstructure evolution were determined using a JEOL JEM-2100FX transmission electron microscope (TEM) and a Quanta 600 field-emission-gun scanning-electron microscope (FEG SEM). EBSD was conducted in a FEI Nova NanoSEM 450 FEG SEM equipped with a Hikari EBSD detector and a TSL OIM™ system version 6.0. EBSD maps of heavily deformed titanium alloy may

contain a number of pixels with low confidence index (CI); the pixels with  $\text{CI} < 0.1$  (for the  $\alpha$  phase) or  $\text{CI} < 0.06$  (for the  $\beta$  phase) were excluded from consideration.

The dislocation density was determined by counting the individual dislocations within the grains/subgrains; the standard deviation was calculated using at least eight arbitrarily-selected TEM images for each sample. The linear-intercept method was used to determine the mean size of the (sub)grains or particles. To avoid uncertainties in the identification of the position of (sub)grain or particle boundaries, some images of the same area were taken at different sample stage angles.

The microstructures developed in both the gage section and (un-deformed) shoulders of each specimen were examined to determine the mechanisms and kinetics of dynamic and static microstructural changes, respectively.

## 3. Results

### 3.1. Initial microstructure

Usually the microstructure of two-phase titanium alloys such as Ti–6Al–4V consists of  $\alpha$  particles with a globular or lamellar morphology lying within a continuous  $\beta$  matrix. Due to the rather low volume fraction of the  $\beta$  phase in Ti–6Al–4V at low temperatures (<10% at 550 °C) and the very large deformation which was used to manufacture the program material, the matrix phase in the present work (and related efforts [16,17]) appears to have changed from  $\beta$  to  $\alpha$ . That is to say, the  $\alpha$  phase looked like a continuous matrix with a typical grain structure while the  $\beta$  phase was usually imbedded at triple junctions between the  $\alpha$  phase (Fig. 1). However, the appearance of the  $\beta$  phase as discrete particles could have been an artifact associated with 2D observations. In this regard, recent investigations [18,19] have shown that a phase which is seen on a cross-section as separate particles may indeed be continuous, but branched. After large deformation, the  $\beta$  phase, being initially the matrix, could thus have remained continuous even with its very low fraction and existed as both equiaxed particles (at triple junctions) and very thin layers between  $\alpha$  particles.

For the description of the evolution of the microstructure in heavily-deformed Ti–6Al–4V, attention was focused on several key features (Fig. 1a): (i)  $\alpha$  or  $\beta$  particles which were delineated by  $\alpha/\beta$  interphase boundaries and surrounded by the other phase and (ii)  $\alpha$  or  $\beta$  (sub)grains which were surrounded by the same phase and delineated by  $\alpha/\alpha$  or  $\beta/\beta$  (sub)boundaries, respectively. The (sub)grains of  $\alpha$  or  $\beta$  lay within  $\alpha$  or  $\beta$  particles, respectively; for the present material, almost no (sub)boundaries were observed in the  $\beta$  phase, thereby suggesting that its microstructure comprised essentially a collection of particles. Classical models describing microstructure instabilities such as grain growth or coarsening during heat treatment or warm/hot deformation typically deal with single-phase grains (sometimes pinned by a small volume fraction of particles) or a small to moderate volume fraction of second-phase particles in a continuous matrix phase. In the present case, on the other hand, a large fraction of the  $\alpha$  (sub)grains have a portion of their boundary lying on the periphery of  $\alpha$  particles; thus a number of  $\alpha$  grains are delineated by both  $\alpha/\alpha$  and  $\alpha/\beta$  boundaries. The migration of (sub)grain and interphase boundaries is described by different expressions, thus complicating the analysis of microstructure evolution.

TEM examination revealed that the microstructure of the program alloy after MF and rolling at 475 °C (hereafter referred to as the initial one), consisted of both  $\alpha$  and  $\beta$  phases micro-constituents with a mean size of the visible fragments ( $\alpha$  (sub)grains and  $\beta$  particles) with different contrast of 0.1–0.4  $\mu\text{m}$  (Fig. 2a). Grain and (sub)grain boundaries were often masked by multiple dislocation

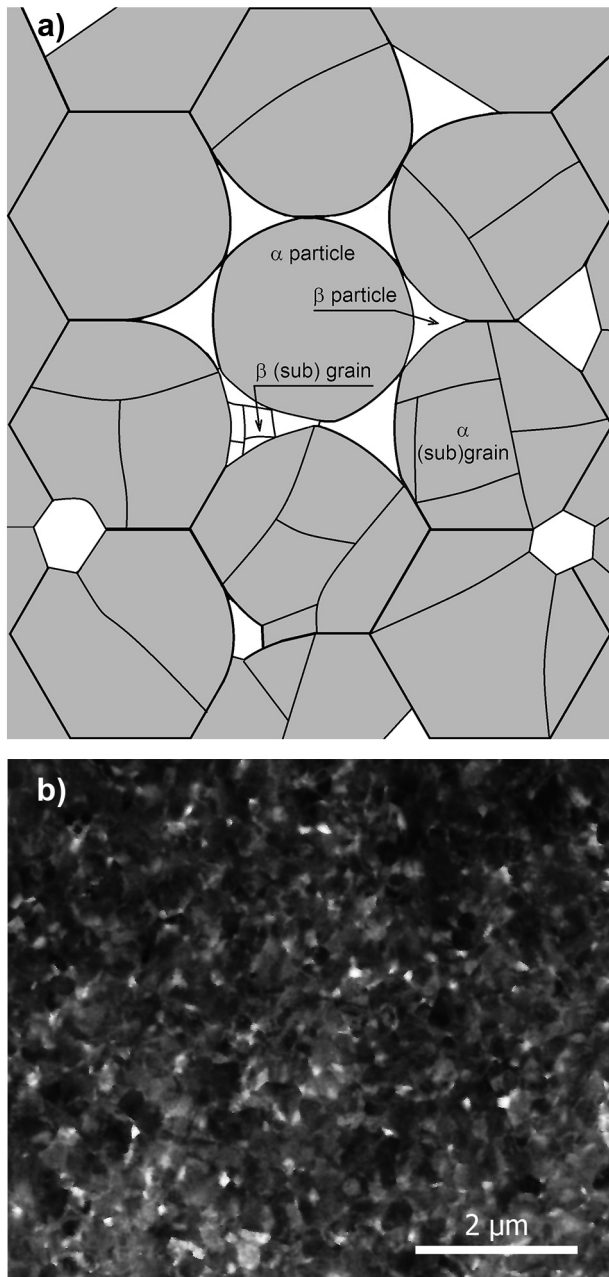


**Fig. 1.** Microstructure of ultrafine Ti–6Al–4V produced by large deformation at low temperatures: (a) Schematic illustration of the possible distribution of the  $\alpha$  and  $\beta$  phases and microstructural constituents and (b) backscattered electron (BSE) image of the microstructure following a heat treatment comprising 0.4 h at 550 °C. In (b), the  $\alpha$  phase is dark, and  $\beta$  is light.

pile-ups and extinction contours. A histogram of the  $\alpha$ -phase (sub) grain size (Fig. 2b) suggested a typical distribution in terms of shape and the ratio of the maximum to mean size (i.e.,  $\sim 2.5$ ), often found for single-phase alloys which have undergone discontinuous static (or dynamic) recrystallization.

### 3.2. Static coarsening

TEM revealed that heat treatment at 550 °C for 100 h resulted in a decrease in dislocation density ( $\rho$ ) and the disappearance of some pile-ups and sub-boundaries (Fig. 3a). The latter resulted in a considerable increase in the size of  $\alpha$  (sub)grains. After long-time

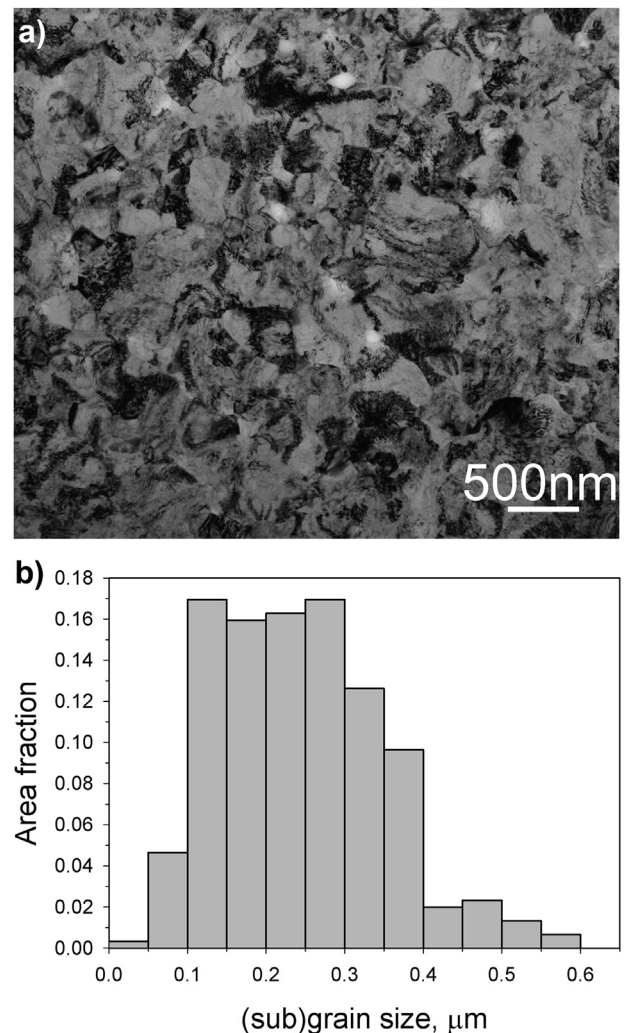


**Fig. 2.** Microstructure of Ti–6Al–4V in the initial condition (after MF and rolling): (a) TEM bright-field image and (b)  $\alpha$ -phase (sub)grain-size distribution.

annealing, the subgrains grew more than twice in size (Table 1). The decrease in  $\rho$  occurred rather quickly during the initial stages of annealing at 550 °C (i.e., during the initial 3.5 h) and then became slower;  $\rho$  was reduced to  $2.5 \times 10^{14} \text{ m}^{-2}$  after 100 h (Fig. 3b). Furthermore, the maximum soak time at 550 °C (100 h) resulted in the formation of a microstructure consisting of  $\beta$  particles and  $\alpha$  (sub)grains having rather low dislocation density and well-distinguished boundaries (Fig. 3a).

During annealing at 550 °C, SEM and EBSD analysis revealed only modest growth of  $\alpha$  and  $\beta$  particles (Fig. 4). After 100 h at this temperature, the globular- $\alpha$  particles were 0.1–1  $\mu\text{m}$  in diameter with a mean value of 0.43  $\mu\text{m}$  (Fig. 4a). There were almost no sub-boundaries within the particles of the  $\alpha$  phase, thus suggesting that certain  $\alpha$  (sub)grains had grown in size to those of their respective particles in which they lay (Table 1). Uniformly-distributed, equiaxed particles of the  $\beta$  phase (Fig. 4b) appeared not to form a continuous network; however, EBSD analysis could neither confirm nor disprove this observation because of limited resolution in regions near  $\alpha/\alpha$  or  $\alpha/\beta$  boundaries. The (0002)  $\alpha$  phase pole figure (insert in Fig. 4a) consisted of basal poles somewhat uniformly distributed along the transversal direction (TD) and slightly split toward the rolling direction (RD). Qualitatively, the same texture for this material was obtained by X-ray analysis in Ref. [8] for the initial condition and after annealing at 550 °C for 0.5 h.

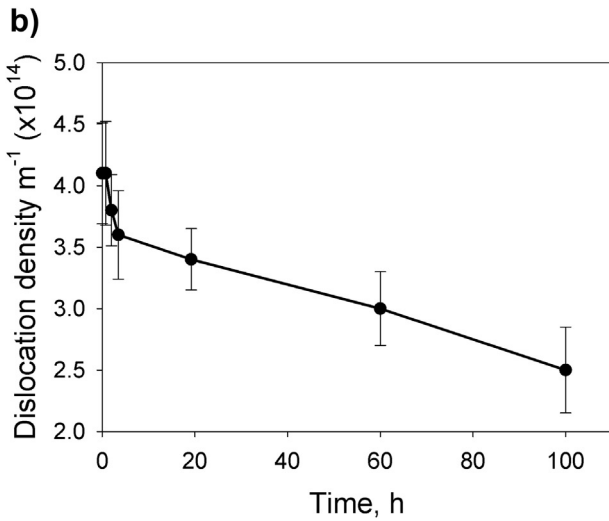
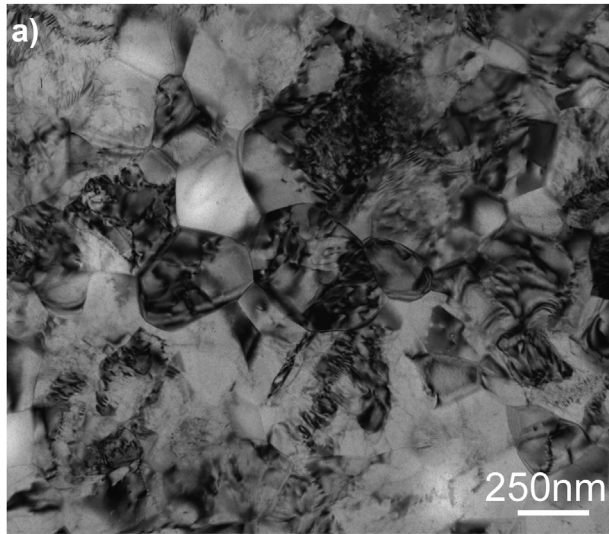


**Fig. 3.** Microstructure of the ultrafine Ti–6Al–4V after annealing at 550 °C: (a) TEM for a sample heat treated for 100 h and (b) dislocation density as a function of time.

**Table 1**  
Measured and predicted sizes of  $\alpha$  (sub)grains ( $d_\alpha$ ),  $\alpha$  particles ( $D_\alpha$ ), and  $\beta$  particles ( $D_\beta$ ) in ultrafine Ti–6Al–4V after annealing at  $T = 550$  °C.

Time (h)	$d_\alpha$ ( $\mu\text{m}$ )	$D_\alpha$ ( $\mu\text{m}$ )	$D_\beta$ ( $\mu\text{m}$ )	$f_\beta$ (Pct.)	$D_\alpha = 4r_\beta/3f_\beta$	$r_\alpha f_\beta/r_\beta$
0	0.14	0.24	0.11	3.5	2.36	0.067
0.75	0.17	0.25	0.12	3.6	2.42	0.069
2.0	0.24	0.25	0.13	4.0	2.28	0.073
3.5	0.26	0.26	0.15	3.9	2.63	0.066
10.0	0.28	0.28	0.16	3.4	2.96	0.063
19.2	0.30	0.30	0.18	3.8	3.16	0.063
60	0.32	0.38	0.25	4.1	4.06	0.062
100	0.38	0.43	0.28	3.7	4.34	0.066

In earlier work [16], the coarsening of  $\alpha$  particles was shown to be accompanied by a simultaneous increase in the size of  $\beta$  particles. The relationship between the diameter ( $D_\alpha$ ) of the pinned phase (which is supposed to be the  $\alpha$  phase in the present case) and the radius ( $r_\beta$ ) and volume fraction ( $f_\beta$ ) of the pinning phase was described using a Zener-like relation [20] of the following form:  $r_\alpha = Cr_\beta/f_\beta$ . For classic Zener behavior, pertinent to the pinning of grains by a small volume fraction ( $\leq 0.01$ ) of particles, the value of  $C$  is  $2/3$  (0.67). For the present observations, a near-linear relation

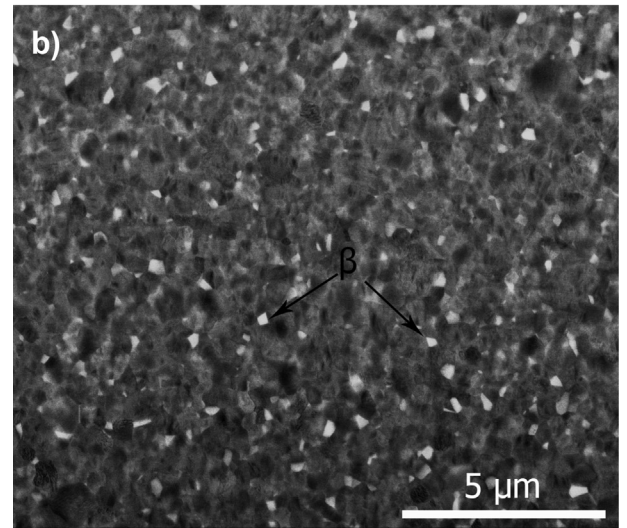
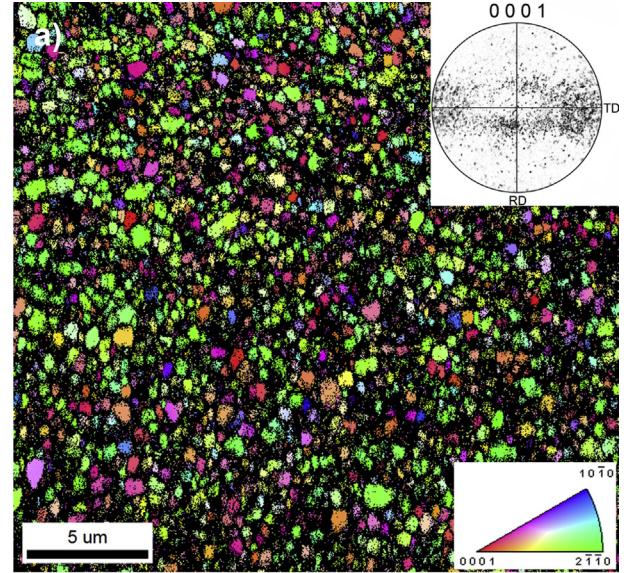


**Fig. 4.** (a) EBSD inverse-pole-figure (IPF) map of the  $\alpha$  phase (+the corresponding  $(0002)_\alpha$  pole figure and color key for the IPF map) and (b) BSE image of the ultrafine Ti–6Al–4V after annealing at 550 °C for 100 h. The EBSD map is shown in the as-scanned condition for points with a confidence index greater than 0.1. (For interpretation of the references to colour in this figure legend, the reader is referred to the web version of this article.)

between  $r_\alpha$  and of  $r_\beta/f_\beta$  was indeed found for the samples annealed at  $T = 550$  °C (Fig. 5a); the slope  $C$  was equal to 0.06. The calculated values of  $C = r_\alpha f_\beta/r_\beta$  fell in the interval of 0.062–0.076 (Table 1). These values of  $C$  are almost an order of magnitude lower than that for classic Zener behavior (0.67). Similarly, the predicted sizes of the  $\alpha$  particles ( $D_\alpha = 4r_\beta/3f_\beta$ ) were an order of magnitude larger than the measured sizes (Table 1).

The broad trend of decreasing of  $r_\alpha f_\beta/r_\beta$  with a decrease in annealing temperature (and volume fraction of beta) was observed earlier [16]. In particular, the value of  $r_\alpha f_\beta/r_\beta$  at 650 °C was found to be  $\sim 0.2$  in comparison to 0.39–0.53 at 775–900 °C. In plotting the previous and current data together, the dependence of  $r_\alpha f_\beta/r_\beta$  on annealing temperature was in fact linear (Fig. 5b). According to this trend, the value of  $C$  would become zero at  $\sim 500$  °C, thus corresponding to the temperature below which Zener-like behavior is not observed in Ti–6Al–4V.

In earlier work [16,21], the kinetics of static coarsening of  $\alpha$  particles in Ti–6Al–4V during annealing at temperatures between

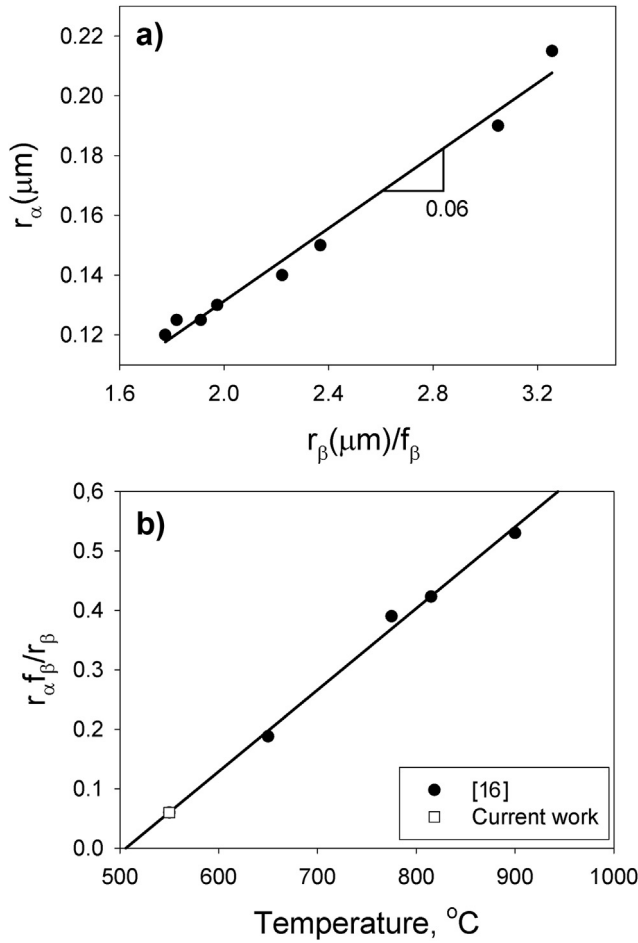


**Fig. 5.** (a) Relation between the  $\alpha$  and  $\beta$  particle sizes in Ti–6Al–4V during static annealing at 550 °C for 0–100 h and (b) the value of  $r_{\alpha}f_{\beta}/r_{\beta}$  as a function of annealing temperature; the average values of  $r_{\alpha}f_{\beta}/r_{\beta}$  for 650–900 °C in (b) were taken from Ref. [16].

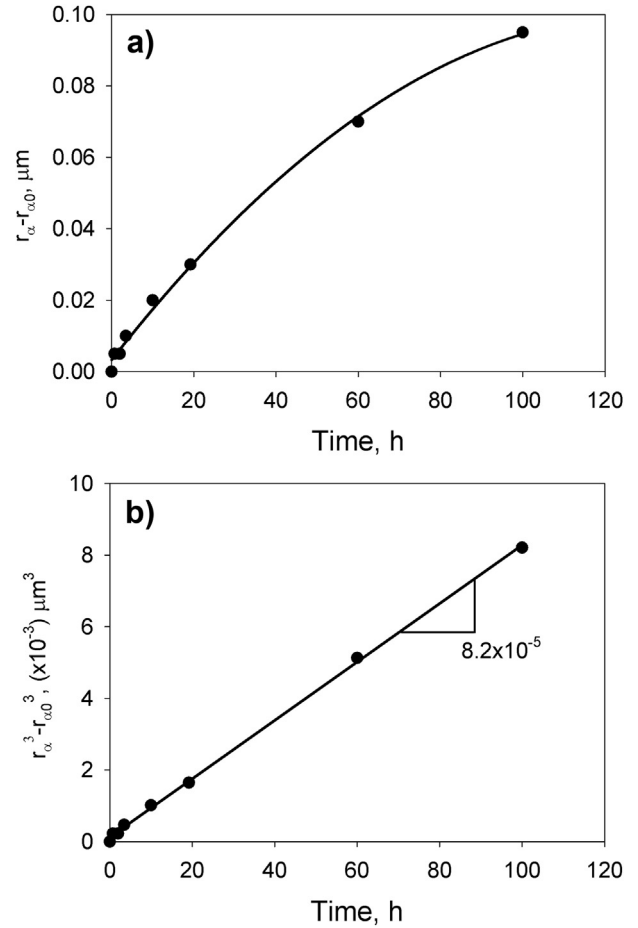


**Fig. 6.** Plots of (a)  $r_{\alpha} - r_{\alpha 0}$  and (b)  $r_{\alpha}^3 - r_{\alpha 0}^3$  vs time at 550 °C for ultrafine Ti–6Al–4V.

650 and 955 °C were interpreted in terms of a modified Lifshitz-Slyozov-Wagner (MLSW) relation of the form:  $r_{\alpha}^n - r_{\alpha 0}^n = K_{MLSW}(t - t_0)$  in which  $n = 3$  and  $K_{MLSW}$  is the coarsening-rate constant. The value of  $n = 3$  suggested that coarsening of the  $\alpha$  phase was limited by solute diffusion through the  $\beta$  matrix. In the present work, the static coarsening of the  $\alpha$  particles (Fig. 6a) was also approximated by a straight-line fit when plotted in terms of  $r_{\alpha}^3 - r_{\alpha 0}^3$  vs.  $t$  with  $n = 3$  (Fig. 6b).

The applicability of the MLSW model was evaluated further by a comparison of measured and predicted rate constants. The form of the theoretical rate constant,  $K_{MLSW}$ , for a finite volume fraction of particles in a system comprising two concentrated alloy phases is the following [21]:

$$K_{MLSW} = \frac{8f(\phi)D\gamma_{\alpha\beta}C_{\beta}(1 - C_{\beta})V_M}{9RT(C_{\alpha} - C_{\beta})^2 \left[ 1 + \partial \ln r / \partial \ln C_{\beta} \right]}, \quad (2)$$

in which  $f(\phi)$  describes the functional dependence of the rate constant on volume fraction  $\phi$ ,  $D$  denotes the diffusivity in the beta matrix of the rate-limiting solute,  $\gamma_{\alpha\beta}$  is the energy associated with particle-matrix (alpha-beta) interfaces (in J/m<sup>2</sup>),  $C_{\alpha}$  and  $C_{\beta}$  are the equilibrium concentrations in the  $\alpha$  particle or beta matrix, respectively, of the rate-limiting solute (expressed as an atomic fraction),  $V_M$  is the molar volume of the precipitate,  $R$  is the

universal gas constant, and  $T$  is the absolute temperature and  $r$  is the activity coefficient of the rate-limiting solute in the beta matrix. As shown in Ref. [21], the diffusion of vanadium through the  $\beta$  matrix is rate limiting in comparison to the diffusion of aluminum.

Input data required to calculate the coarsening rate constant comprise the molar volume of the  $\alpha$  particles  $V_M = 10440 \text{ mm}^3$ , the  $\alpha/\beta$  surface energy, taken here to be  $\gamma_{\alpha\beta} = 0.26 \text{ J/m}^2$  per Ref. [22]. The thermodynamic factor for vanadium solutes in  $\beta$  titanium and the volume fraction function were taken to be equal to  $\sim 1$  and  $\sim 4$ , respectively [21,23]. Based on the data reported in Refs. [16,21], the composition term (i.e.,  $C_{\beta}(1 - C_{\beta})/(C_{\alpha} - C_{\beta})^2$ ) at 550 °C was taken to be  $\sim 5.5$ . The measured diffusivities of vanadium in the  $\beta$  phase were calculated from the expression  $D_{\beta}^V (\mu\text{m}^2/\text{s}) = 77000 \exp(-17460/T(K))$  [21], thereby yielding a diffusivity of  $4.7 \times 10^{-5} \mu\text{m}^2/\text{s}$  at 550 °C. The predicted value of the coarsening rate  $K_{MLSW}$  was thus found to be  $1.1 \times 10^{-3} \mu\text{m}^3/\text{h}$ , which is approximately an order of magnitude larger than the measured value (Fig. 6b). Based on this comparison, it thus appears that the MLSW model should be viewed as somewhat approximate for the regime of low temperature and high volume fraction of particles investigated in the present work.

In order to check the hypothesis regarding the persistence of thin  $\beta$  layers in the microstructure, a specimen of ultrafine Ti–6Al–4V was annealed at 550 °C for 10 h and examined using energy-dispersive (X-ray) spectroscopy (EDS). The increased concentration of V found along an  $\alpha/\alpha$  boundary (indicated by the arrow in Fig. 7a) suggested either an increased grain-boundary diffusivity of V or the presence of a very thin  $\beta$  layer between

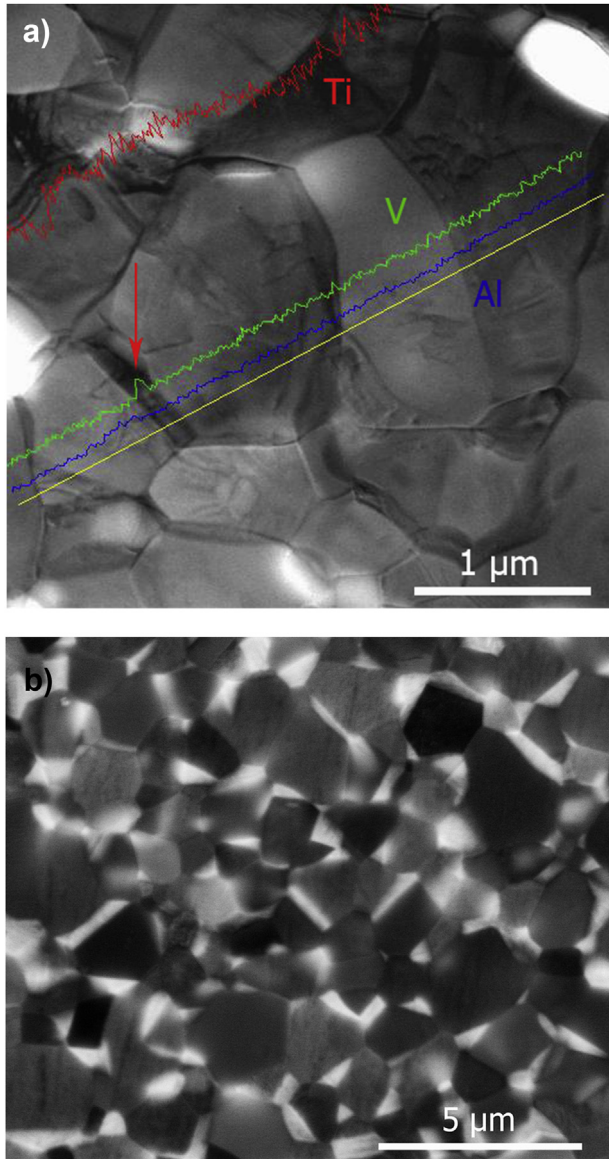


**Fig. 7.** (a) EDS measurements of the distribution of chemical elements (Ti, V, Al) along a straight line in a specimen annealed at 550 °C for 10 h and (b) BSE image of microstructure developed in ultrafine Ti–6Al–4V during annealing at 815 °C for 15 min.

those  $\alpha$  (sub)grains. The latter suggestion may be plausible taking into account the usual control of coarsening kinetics by the diffusion of vanadium. On the other hand, the rapid transformation of equiaxed  $\beta$  particles situated at triple junctions of  $\alpha$  grains during a short exposure time (15 min) at 815 °C into plate-like  $\beta$  layers can also be associated with the pre-existence of  $\beta$  between some  $\alpha/\alpha$  boundaries.

### 3.3. Dynamic coarsening

Coarsening of the ultrafine Ti–6Al–4V microstructure during superplastic deformation was found to be much more pronounced in comparison with that during static annealing at an equivalent temperature (Fig. 8, Table 2). During superplastic deformation at 550 °C and  $2 \times 10^{-4} \text{ s}^{-1}$ , for example, the size of (sub)grains of the  $\alpha$  phase and particles of the  $\beta$  phases increased continuously. Moreover, their boundaries became less distorted and more-sharply

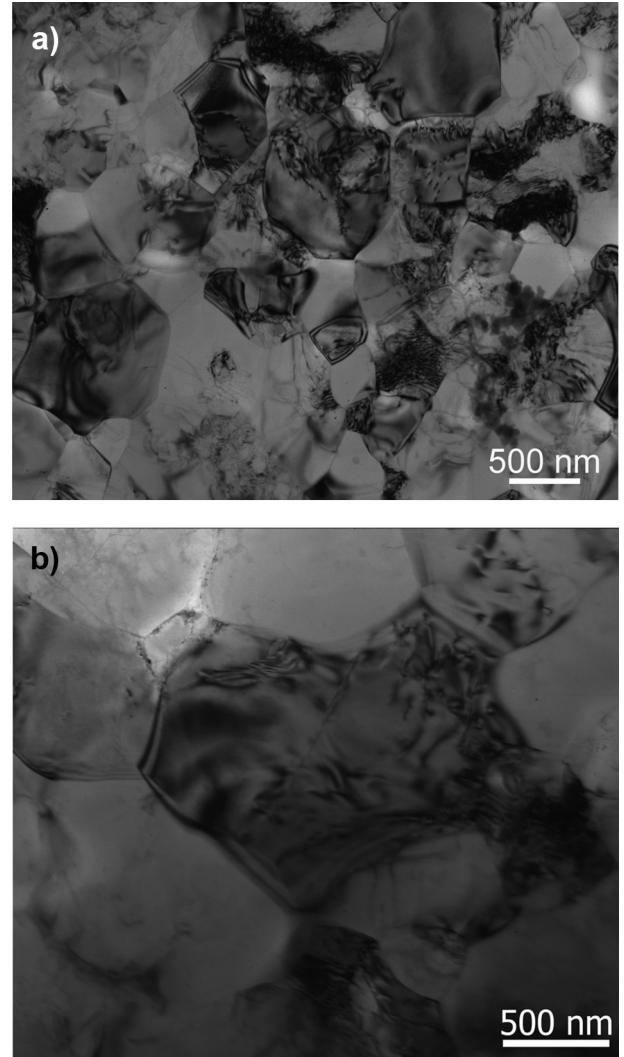


**Fig. 8.** TEM micrographs for ultrafine Ti–6Al–4V after superplastic flow at 550 °C/  $2 \times 10^{-4} \text{ s}^{-1}$  to an elongation of (a) 200% or (b) 800%. The tension axis was vertical in both cases.

**Table 2**

Measured and predicted sizes of  $\alpha$  and  $\beta$  particles in ultrafine Ti–6Al–4V after superplastic deformation at 550 °C and  $2 \times 10^{-4} \text{ s}^{-1}$ .

Elong. (%)	Time (h)	$D_\alpha$ (μm)	$D_\beta$ (μm)	$f_\beta$ (Pct)	$D_\alpha = 4r_\beta/3f_\beta$	$r_\alpha f_\beta/r_\beta$
0	0	0.24	0.11	3.5	2.09	0.08
100	2.0	0.57	0.23	3.9	3.93	0.09
200	4.3	0.73	0.29	4.1	4.72	0.10
500	9.9	0.98	0.36	4.3	5.58	0.12
800	17.3	1.15	0.42	4.5	6.22	0.13

delineated. In addition, the dislocation density  $\rho$  decreased noticeably as a result of deformation (Fig. 9). The steady decrease in  $\rho$  was observed until an elongation of 500% (Fig. 9a); further deformation was not accompanied by a noticeable change in  $\rho$ . Increasing the strain rate at 550 °C resulted in an increase in  $\rho$  (measured at 100% elongation) (Fig. 9b). It reached a level comparable to that in the initial condition for a strain rate of  $5 \times 10^{-2} \text{ s}^{-1}$ . However, the results did show a local plateau in dislocation density for strain rates between  $2 \times 10^{-4}$  and  $10^{-3} \text{ s}^{-1}$ .

EBSD analysis also showed a considerable increase in the size of the  $\alpha$  particles during superplastic deformation at 550 °C and

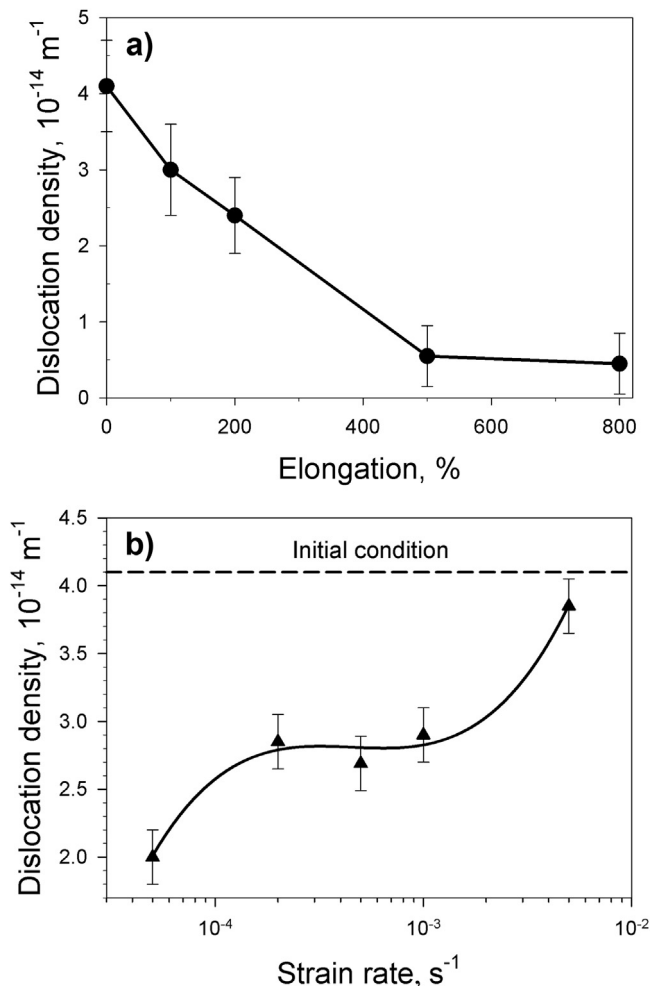


**Fig. 9.** Dislocation density developed in ultrafine Ti–6Al–4V during superplastic flow at 550 °C as a function of (a) elongation at a strain rate of  $2 \times 10^{-4} \text{ s}^{-1}$  or (b) strain rate for an elongation of 100%.

$2 \times 10^{-4} \text{ s}^{-1}$ ; i.e., to  $\sim 1.2 \mu\text{m}$  after 800% elongation (Fig. 10a). On the other hand, the shapes of the phases following very high elongation remained equiaxed, which is typical of superplasticity at much higher temperatures [1,2]. Moreover the (0002) $_{\alpha}$  pole figure (insert in Fig. 10a) showed a pronounced randomization of the initial texture (insert in Fig. 4a), i.e., a marker of grain/subgrain rotations due to grain-boundary sliding, or one of the main mechanisms of SP deformation. In addition, the  $\alpha$ -phase particles were almost free of substructure. The  $\beta$  phase in SEM images appeared as quite-uniformly distributed particles having a slightly-elongated shape (indicated by the arrows in Fig. 10c). EBSD analysis also suggested that the  $\beta$  phase comprised a continuous network dividing  $\alpha$  particles (Fig. 10b).

Quantitative examination of dynamic-coarsening results was generally in good agreement with conclusions drawn from the static-coarsening behavior quantified at the same temperature (550 °C). The growth of  $\alpha$  and  $\beta$  particles during deformation occurred generally in agreement with a Zener-like model with a value of  $C \approx 0.13$ . The predicted sizes of  $\alpha$  particles were  $\sim 5$ – $10$  times larger than the measured values (Table 2). The coarsening of the  $\alpha$  phase was also described by the relation  $r^n - r_0^n = f(t)$  with the best fit for  $n = 3$  (Fig. 11).

As expected, a comparison of coarsening rates (Figs. 6b and 11) showed that the dynamic value was greater than the static one; i.e.,

by approximately two orders of magnitude. According to the previous high-temperature observations [16], this increase can be ascribed to enhanced diffusion associated with the generation of dislocation substructure in the  $\beta$  phase through which solutes are being transported. The factor by which diffusion was enhanced during low-temperature deformation, however, was somewhat greater than that observed previously for higher-temperature deformation, i.e., 4 to 10, and may be associated with redistribution of the  $\beta$  phase in the structure (from triple junctions to interfaces between  $\alpha$  particles) during superplastic flow.

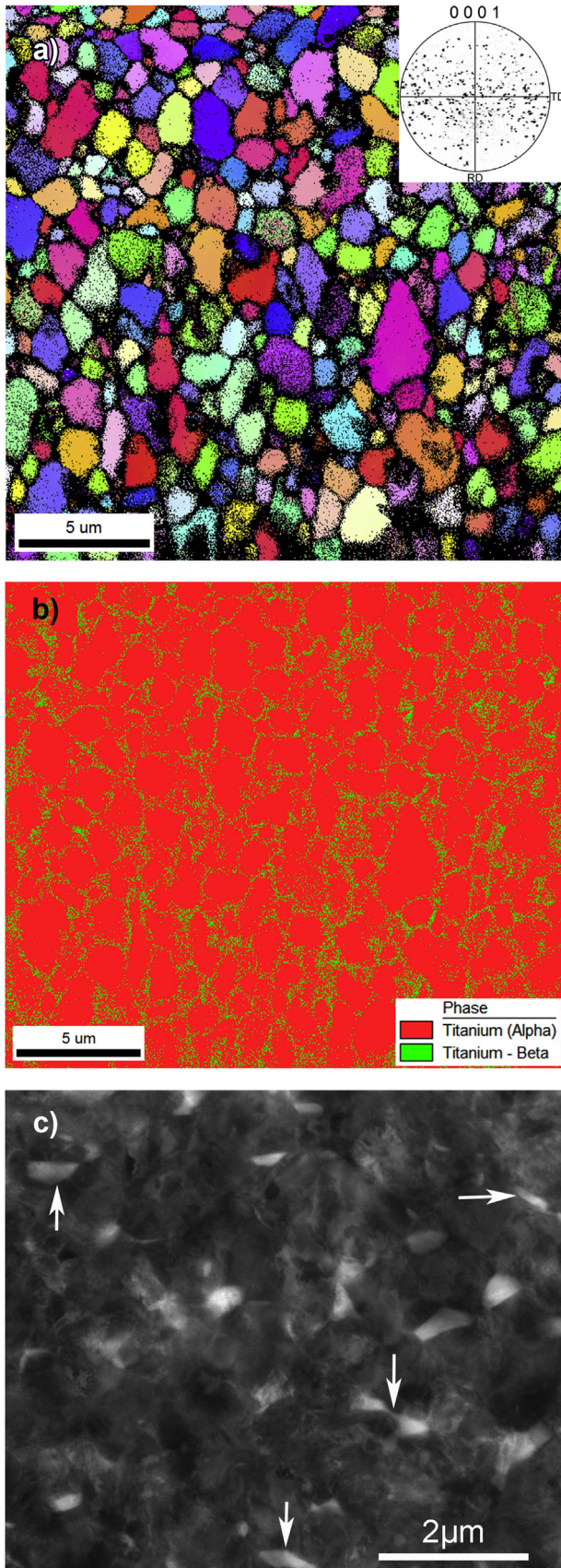
### 3.4. Superplastic behavior

Fig. 12 summarizes the mechanical properties of the ultrafine alloy as a function of temperature and strain rate. An increase in deformation temperature increased the ductility and resulted in a marked decrease in flow stress (Fig. 12a). At  $T = 550^\circ\text{C}$  and  $\dot{\epsilon} = 5 \times 10^{-4} \text{ s}^{-1}$ , the total elongation was  $\sim 810\%$ . A further increase in temperature led to a small increase in elongation, a trend likely mitigated by oxidation and the formation of an alpha case. An examination of specimens strained at different temperatures showed that deformation at 550 °C occurred most homogeneously. The effect of strain rate on the mechanical behavior at 550 °C was also typical of that for superplastic deformation (Fig. 12b). The optimal SP parameters for the ultrafine alloy were thus  $T = 550^\circ\text{C}$  and a strain rate of  $2 \times 10^{-4} \text{ s}^{-1}$  which resulted in  $\delta \approx 1000\%$  and  $m = 0.43$ .

The shapes of the flow curves for the ultrafine material at  $T = 550^\circ\text{C}$  showed a noticeable dependence on strain rate (Fig. 13a). At  $2 \times 10^{-3} \text{ s}^{-1}$ , the flow curve exhibited a peak flow stress at the initial stages of deformation followed by pronounced flow softening. A decrease in strain rate to the optimal value of  $2 \times 10^{-4} \text{ s}^{-1}$  changed the mechanical behavior to a marked flow-hardening response suggestive of dynamic coarsening [5]. A similar behavior was observed at the yet lower strain rate of  $2 \times 10^{-5} \text{ s}^{-1}$ . In general, such behaviors are typical of SP flow. However, there were large differences in the levels of flow stress. For the optimal condition at  $2 \times 10^{-4} \text{ s}^{-1}$ , the flow stress was 150–200 MPa. This is approximately an order of magnitude higher than that typically observed for high-temperature superplasticity at the same strain rate [1]. Such high flow stresses can limit the application of superplastic (blow) forming at this very low temperature because the amount of pressure at which this manufacturing technique is typically performed may not be sufficient. However, the results of [3] do demonstrate the applicability of blow forming at 600 °C for ultrafine Ti–6Al–4V.

Additional insight into the mechanism of plastic flow was provided by measurements of the strain-rate sensitivity of the flow stress ( $m$  value). The value of  $m$  showed a noticeable dependence on strain (Fig. 13b). For the strain-rate range between  $2 \times 10^{-4}$  and  $5 \times 10^{-4} \text{ s}^{-1}$ , the  $m$  value increased with deformation from 0.39 to 0.48. The most rapid increase occurred during the beginning of deformation and then became less pronounced. The simultaneous increase in both the  $m$  value and flow stress with strain may be associated with the complex interactions of dynamic coarsening and a transition of sliding along boundaries which are mainly  $\alpha/\alpha$  to those which are primarily  $\alpha/\beta$  due to transformation of the  $\beta$  phase into being the matrix during deformation.

The magnitude of the flow stress  $\sigma$  and the  $m$  value of the ultrafine Ti–6Al–4V was interpreted in terms of the Bird–Mukherjee–Dorn generalized constitutive relation (Eq. (1)), which was rearranged to obtain an expression for the product of the two unknown quantities,  $AD$ ; viz.



**Fig. 10.** (a) EBSD inverse-pole-figure maps of the  $\alpha$  (+the corresponding  $(0002)_{\alpha}$  pole figure; the color key is the same as in Fig. 4a), (b) color-coded phase map, and (c) BSE image of the ultrafine Ti–6Al–4V after superplastic deformation at 550 °C/ $2 \times 10^{-4} \text{ s}^{-1}$

$$AD = \left( \frac{\dot{\epsilon} k T}{G b} \right) \left( \frac{G}{\sigma} \right)^n \left( \frac{d}{b} \right)^p \quad (3)$$

Values of the right-hand side of Eq. (3) were calculated using measurements of  $\sigma$  and  $d = D_{\alpha}$  for an elongation of 800% (Table 2, Fig. 13a) at a strain rate of  $2 \times 10^{-4}$  and  $T = 550$  °C, assuming  $n = 2.1$  ( $\approx 1/0.48$ , where 0.48 is the corresponding  $m$  value at the end of the superplastic tension test, Fig. 13b). This value of the stress exponent  $n$  indicated that GBS was likely accommodated by dislocation glide-climb, which would yield  $n = 2$ .

Quantitative models to describe superplastic flow accommodated by slip processes have also been developed by Ball and Hutchinson [24], Mukherjee [25], and Langdon [26]. In these models, stress concentrations developed at triple points due to grain-boundary sliding are assumed to be accommodated by climb-limited glide of dislocations either into or along the grain boundaries. However, descriptions of superplastic deformation in two-phase alloys are complicated by the different properties of the two phases as well as the presence of interphase and intergranular boundaries. For  $\alpha/\beta$  titanium alloys in which the two phases exhibit noticeably-different deformation behavior and rates of bulk diffusion, the core-mantle model proposed by Gifkins [27] seems more suitable. In particular, good agreement of the Gifkins model with experimental observations was noted in Ref. [16] for low-temperature superplastic flow of ultrafine Ti–6Al–4V.

In the Gifkins model, each grain consists of a core region surrounded by a deformable mantle of variable width. Stress concentrations developed at triple points due to GBS are assumed to be accommodated by climb-limited glide of dislocations in the vicinity of grain boundaries (i.e., mantle regions) or diffusional flow either through the grains or along the grain boundaries. The interpretation of the low-temperature superplastic behavior of two-phase titanium alloy in terms of the core-mantle model [16] suggested that the  $\alpha$  phase was the core (the core size was taken to be the alpha particle size  $D_{\alpha}$ ) and the other parameters were based on the properties of the mantle (which was taken to be the  $\beta$  regions surrounding the alpha particles).

The grain-size exponent of the strain rate ( $p$ ) was determined to be  $\sim 1.8$  by applying the relation  $p = n[\log(\sigma_2/\sigma_1)]/[\log(r_{\alpha 2}/r_{\alpha 1})]$ , in which the flow stresses ( $\sigma$ ) and  $\alpha$  particle radii ( $r_{\alpha}$ ) were evaluated at elongations of 100 and 800% (Table 2, Fig. 13a). The value of  $p \approx 2$  also corresponds to GBS accommodated by matrix dislocation motion.

Other material properties in Eq. (3) as well as  $\log(AD)$  data for temperatures between 650 and 955 °C were taken from Ref. [16]: the value of  $G \sim 20$  GPa was taken to be the shear modulus of  $\beta$  titanium; the length of the Burgers vector  $b$  was assumed to be that for unalloyed  $\beta$  titanium (0.287 nm). The temperature dependence of  $G$  was neglected based on ultrasonic measurements of Young's modulus, which indicated very little effect of temperature for the  $\beta$  phase [28]. As shown in Fig. 14a, the value of  $\log(AD)$  for 550 °C and  $2 \times 10^{-4} \text{ s}^{-1}$  fell rather close to the trend line obtained in Ref. [16] for higher temperatures. This suggested that the core-mantle model can still be applied to superplastic flow at the very low temperature of 550 °C.

The apparent activation energy found in Refs. [16,29] ( $Q = 160$  kJ/mol) was very close to that calculated in the present work from a plot of  $\ln(\sigma/G)$  vs.  $1/T$ . For the optimal parameters of

to 800% elongation. The IPF map is shown in the as-scanned conditions for points with a confidence index  $CI > 0.1$ . The tension directions were vertical in all cases. (For interpretation of the references to colour in this figure legend, the reader is referred to the web version of this article.)

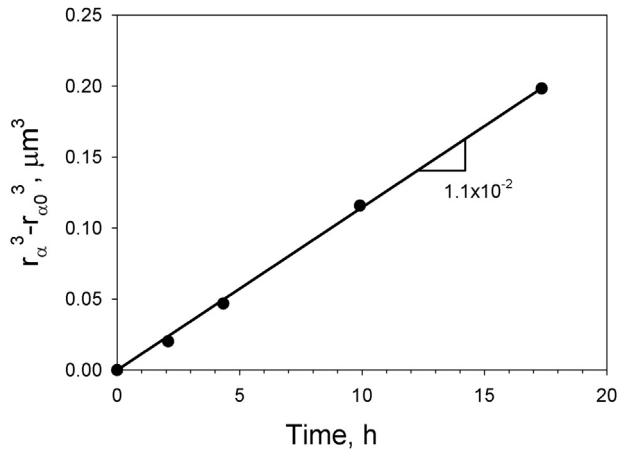


**Fig. 11.** Plot of  $r_\alpha^3 - r_{\alpha 0}^3$  vs. time during superplastic deformation of ultrafine Ti–6Al–4V at 550 °C and  $2 \times 10^{-4} \text{ s}^{-1}$ .

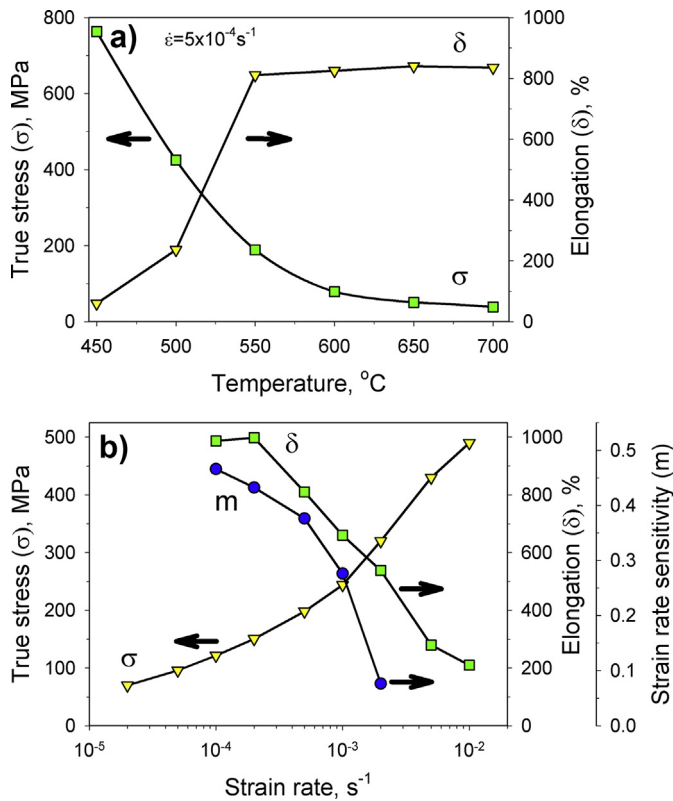


**Fig. 12.** Mechanical properties of ultrafine Ti–6Al–4V as a function of (a) deformation temperature at  $\dot{\epsilon} = 5 \times 10^{-4} \text{ s}^{-1}$  and (b) strain rate at  $T = 550^\circ\text{C}$ . The stress level was defined at  $\epsilon \sim 0.2$ .

superplasticity,  $Q = 151 \text{ kJ/mol}$  and  $n \approx 2$  were obtained (Fig. 14b). In an earlier work for the same alloy [6], a similar value of  $Q = 176 \text{ kJ/mol}$  for region II (superplastic) flow was determined for  $T = 600^\circ\text{C}$ . These values of activation energy are close to that determined for the bulk diffusivity of vanadium and aluminum in beta titanium (145 and 150 kJ/mol, respectively) [30] and for self-diffusion in beta titanium (131–153 kJ/mol) [31–33] at temperatures between  $900^\circ\text{C}$  and  $1540^\circ\text{C}$ . Thus, it might be hypothesized that the deformation mechanism operating at lower temperatures for the UFG Ti–6Al–4V is indeed GBS accommodated by dislocation glide-climb and, perhaps to a less degree, by solute diffusion.

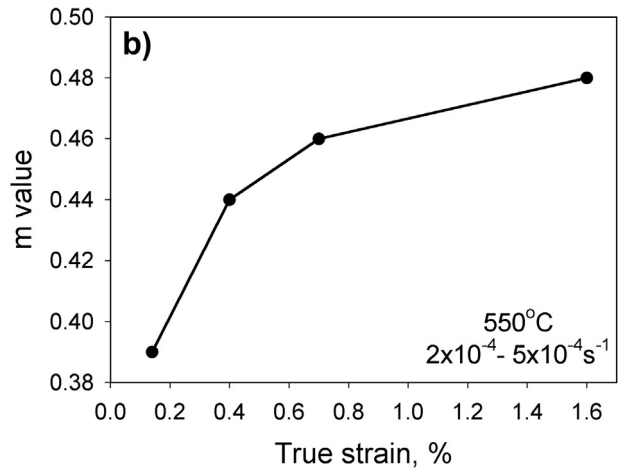
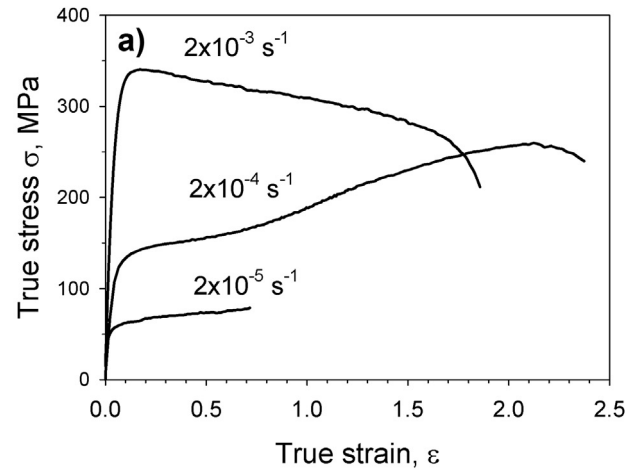


**Fig. 13.** (a) True stress-true strain curves for ultrafine Ti–6Al–4V at  $T = 550^\circ\text{C}$  and various constant strain rates and (b) strain dependence of the m value at  $550^\circ\text{C}$  determined from strain-rate jump tests.

### 3.5. Porosity

The ultrafine microstructure of the present Ti–6Al–4V material was also found to be beneficial in retarding the formation of porosity during low-temperature superplastic flow. A few isolated voids were observed in the vicinity of the fracture surface of specimens tested at  $600^\circ\text{C}$  and a strain rate  $5 \times 10^{-4} \text{ s}^{-1}$ , while there were no cavities whatsoever in a specimen strained at  $550^\circ\text{C}$  and  $5 \times 10^{-4} \text{ s}^{-1}$ . For other strain rates between  $2 \times 10^{-4} \text{ s}^{-1}$  and  $5 \times 10^{-3} \text{ s}^{-1}$  at  $500^\circ\text{C}$ , essentially no porosity was detected metallographically. Measurements of the gage-section density after SP tension tests (based on Archimedes' principle) revealed similar results; i.e., an absence of cavitation within the limits of experimental error.

## 4. Discussion

The present results revealed prominent SP-deformation characteristics for ultrafine Ti–6Al–4V at the extremely low temperature of  $550^\circ\text{C}$ , which is approximately  $400^\circ\text{C}$  lower than the typical SP deformation temperature for this alloy with a much coarser microstructure [1]. In addition to a very high total elongation (1000%) and  $m \approx 0.4$  under optimal SP conditions, the ultrafine alloy demonstrated extremely limited cavitation and a pronounced difference between the kinetics of static and dynamic coarsening. These features are discussed below.

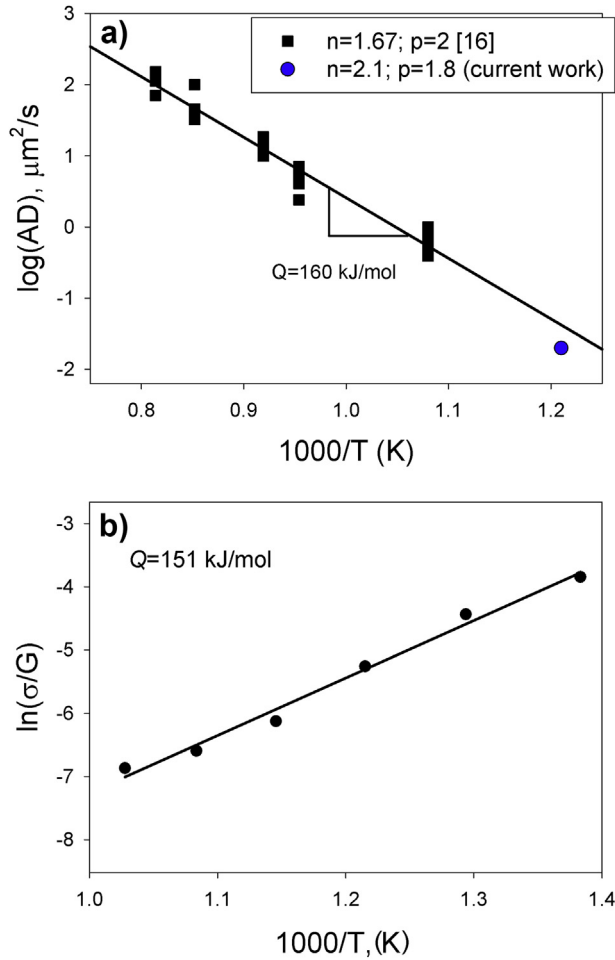


**Fig. 14.** (a) Semilog plot of  $AD$  vs.  $1/T$  used to determine the deformation mechanism during superplastic flow of ultrafine Ti–6Al–4V and (b) semilog plot of  $\sigma/G$  vs.  $1/T$  for the calculation of the apparent activation energy of ultrafine Ti–6Al–4V.

#### 4.1. “Wetting” of $\alpha/\alpha$ boundaries

The observed redistribution of the  $\beta$  phase within the microstructure of the ultrafine Ti–6Al–4V alloy during superplastic flow at 550 °C appears to be an important factor in the development of good mechanical properties, limited cavitation, and the large difference in static vs dynamic microstructural coarsening. Immediately after severe warm working via MF and rolling, the  $\beta$  phase was situated mainly at triple junctions in the form of discrete, equiaxed particles and along some  $\alpha/\alpha$  grain/particle boundaries in the form of very thin layers. After superplastic flow in tension, on the other hand, the  $\beta$  phase appeared to have formed a continuous network separating the  $\alpha$  particles. This transformation of the morphology of the beta phase suggests extensive diffusion along  $\alpha/\alpha$  grains/particle boundaries and may be associated with (i) the called “wetting” effect in the solid state and/or (ii) anisotropy of the interphase boundaries.

The complete or partial wetting of grain boundaries of a high melting point component by a low-melting point phase for various alloys at elevated temperatures (but below the melting point, i.e., when both phases are solid [34]) has been studied in a number of previous works [35,36]. The modes of complete or partial wetting depend on the ratio between the  $\alpha/\alpha$  grain-boundary and  $\alpha/\beta$  interphase-boundary energies ( $\gamma_{gb}$  and  $\gamma_{ib}$ , respectively) [34]. If  $\gamma_{gb} \leq 2\gamma_{ib}$  then the  $\beta$  phase particles tend to reduce their surface area and develop lens-like shapes. If  $\gamma_{gb} > 2\gamma_{ib}$ , the  $\beta$  phase tends to

increase its surface via “wetting” the  $\alpha/\alpha$  boundary. The equilibrium reversible transition between complete and incomplete grain-boundary wetting by a second solid phase has been observed in both Zr- and Ti-based alloys [37–39]. Due to the considerable increase in the energy of grain boundaries  $\gamma_{gb}$ , severe plastic deformation may shift the position of the critical solution/dissolution points towards lower temperatures thereby allowing low-temperature grain-boundary wetting [40,41].

The equilibrium condition between grain boundary and interphase boundary energies  $\gamma_{gb} = 2\gamma_{ib}\cos(\theta/2)$ , in which  $\theta$  is the contact angle, is correct only in case of isotropic interfacial energies and for a stress-free state. By contrast, the interphase energy in two-phase titanium alloys is anisotropic in nature, which may also promote the transformation of the morphology of the  $\beta$  phase from globular to plate-like during long-term annealing [42,43]. The plate-like morphology of  $\beta$  particles may increase the fraction of surfaces with lower energy. However, two points should be taken into account considering the interphase boundary energy in a wrought alloy in comparison with that in a well-annealed colony- $\alpha$  microstructure. First, deformation conditions with an excess of lattice dislocations do not promote the formation of well-organized low-energy  $\alpha/\beta$  interfaces [22]. This factor can be in some degree mitigated during annealing due to recovery processes or during SP flow. Second, neighboring  $\alpha$  particles in a wrought alloy in the most general case have high-angle misorientations. Thus, the  $\beta$  phase can form a low-energy  $\alpha/\beta$  interface with only one  $\alpha$  particle, while the other  $\alpha/\beta$  boundary with the adjacent  $\alpha$  particle most likely would have a higher energy. In the latter case, the interface energy can be decreased by the formation of a series of ledges consisting of low-index planes of both phases [44,45].

The transformation of a near-globular  $\beta$  particle situated at triple junctions of  $\alpha$  particles should be associated with diffusion of V along  $\alpha/\alpha$  boundaries; the net effect of this process is the formation of plate-like  $\beta$  layers between some  $\alpha$  grains. An increased concentration of V was in fact observed along some boundaries as indicated by the arrow in Fig. 7a. Fig. 7b shows a considerable number of  $\alpha/\alpha$  interfaces decorated with  $\beta$  after annealing at 815 °C, thereby corroborating the possible occurrence of “wetting” of  $\alpha/\alpha$  grain boundaries by the  $\beta$  phase.

It was postulated in Ref. [40] that a soft lubricating layer of the second phase (Zn) existing along Al/Al grain boundaries in an Al–Zn alloy facilitates GBS, thereby providing very high ductility. Therefore, a similar effect can be expected for Ti–6Al–4V when layers of the soft  $\beta$  phase are present between  $\alpha$  particles.

#### 4.2. Magnitude of the flow stress

Despite the refined microstructural scale, the higher flow stresses measured in the present work compared to previous measurements can be ascribed largely to the marked decrease in the diffusivity at the lower temperatures utilized and the features of the microstructure. For a Ti–6Al–4V sheet with an  $\alpha$  particle size of  $\sim 2 \mu\text{m}$ , for example, the flow stress at 775 °C and  $2 \times 10^{-4} \text{ s}^{-1}$  was  $\sim 17.5 \text{ MPa}$  [5]. For the present ultrafine material with  $D_\alpha = 0.24 \mu\text{m}$ , the initial flow stress at 550 °C and  $2 \times 10^{-4} \text{ s}^{-1}$  was almost seven times as high, i.e., 130 MPa (Fig. 13a). Such differences can be interpreted in the context of Eq. (1). At a fixed strain rate, rearrangement of this relation yields the following:

$$\sigma = A \left( d^p \left[ T e^{Q/RT} \right] \right)^{1/n}, \quad (4)$$

where  $A$  is a constant. Taking  $D_\alpha = d = 0.24$  and  $2 \mu\text{m}$  at  $T = 550$  and  $775$  °C, respectively,  $n = 2$ ,  $p = 1.8$ , and  $Q = 150 \text{ kJ/mol}$ , the ratio of the flow stresses at a fixed strain rate would be predicted to be 1.4,

not  $130/17.5 \approx 7.4$ . It thus appears that the flow stress estimated from Eq. (4) is quite approximate because the values of  $n$ ,  $p$ , and  $Q$  may depend in some complex fashion on the grain size, the distribution of the phases, and temperature, thereby giving rise to a discrepancy between the predicted and the measured values of flow stress.

Another possible explanation of this result can be associated with the distribution of the  $\beta$ -phase in the microstructure at the beginning of deformation. As mentioned above, the  $\beta$  phase in the initial condition of the microstructure existed as both equiaxed particles at triple junctions and as very thin layers between  $\alpha$  particles. It may be surmised that the thin layers of the  $\beta$  phase are unable to accommodate all of the applied strain, suggesting that the core-mantle model cannot be used for the description of the deformation behavior during the early stage of deformation. After large deformation, on the other hand, the  $\beta$  phase becomes redistributed and forms a rather well-defined, continuous network. At this stage, the  $\beta$  phase divides the  $\alpha$  particles (Fig. 10b) and starts to behave truly as a “mantle”. The applicability of the core-mantle model at the later stages of plastic flow was confirmed by a good correlation of  $\log(AD)$  obtained for the large strain at 550 °C and prior results obtained at higher temperatures (Fig. 14a).

These suggestions are in good agreement with the explanation given in Refs. [46,47] for the “unusual” superplastic behavior of Ti–6Al–4V at 775–825 °C in terms of the general features of the deformation of a composite aggregate of relatively-hard  $\alpha$  grains and softer  $\beta$  grains with different  $\alpha/\beta$  phase ratios and particle sizes.

#### 4.3. Retardation of cavitation

It is well known that a decrease in grain size retards the development of porosity, especially in titanium alloys [1,2]. However, the almost total lack of voids in specimens deformed under superplastic conditions to few hundred percent seems quite unusual. Cavity nucleation is generally a result of the stress concentrations arising from incomplete accommodations of GBS. In particular, stress concentrations are likely to develop at sites such as triple points at which boundary sliding is impeded. Cavities may nucleate if the stress concentrations are not relieved sufficiently rapidly. In ultrafine materials, stress concentrations are relatively weak due to the small mean free length (average space between triple points) associated with GBS. An increase in the critical radius for cavity nucleation  $r_c$  as a result of a decrease in grain size  $D_\alpha$  can be deduced from the following expression [48]:

$$r_c = \frac{2\gamma}{\sigma} - \frac{2D_\alpha\sigma}{3E}, \quad (5)$$

in which  $\gamma$  denotes the surface energy,  $\sigma$  is the remote applied stress, and  $E$  is Young's modulus. In this model, the occurrence of cavitation is associated with the formation of vacancy clusters where dislocation pile-ups meet grain boundaries. However, calculations for the present ultrafine material revealed that the value of  $r_c$  was approximately an order of magnitude smaller than the (sub)grain radius thereby suggesting a rather-high probability for cavity nucleation. In other work, Chokshi [49], using earlier models of Raj [50] and Riedel [51], estimated the critical grain size  $D_{cr}$  for cavity nucleation as

$$D_{cr} \geq \left( \frac{26F_v E \Omega}{kT} \right)^{1/3} \frac{\gamma}{2\sigma}, \quad (6)$$

in which  $F_v$  is a shape factor ( $\approx 1$ ), and  $\Omega$  is the atomic volume ( $\approx 0.7 \text{ b}^3$ ). In the present work the critical (sub)grain size was found to be 40–50 nm for an applied stress  $\sigma = 200 \text{ MPa}$ . Thus,

calculations based on this alternate expression can also not explain why voids were not formed.

The presence of a soft layer (such as  $\beta$ ) between hard grains/particles (of  $\alpha$ ), which is not considered in prior models, may be hypothesized as the primary reason for the suppression of cavitation during superplastic deformation in ultrafine Ti–6Al–4V. The high dislocation density in the warm-worked material, well-developed substructure, and the non-equilibrium condition of grain/interphase boundaries may also promote a high diffusivity (due to both grain boundary and pipe diffusion) and thus relieve stress concentrations via diffusional creep. In addition, the stress-enhanced local diffusivity and high surface energy of the interfaces promoted the coarsening of (sub)grain and particles (Sections 3.2 and 3.3), i.e., boundary migration. This stress-assisted (sub)grain and particle boundary migration would also relieve stress concentrations and possibly reduce the amount of cavitation. These hypotheses warrant additional research, however.

## 5. Conclusions

The low-temperature static- and dynamic-coarsening kinetics and plastic-flow behavior of ultrafine Ti–6Al–4V were established via a series of isothermal tension tests. From this work, the following conclusions were drawn.

1. The deformation behavior of the ultrafine Ti–6Al–4V with a size of  $\alpha$  (sub)grains and  $\beta$  particles between 0.1 and 0.4  $\mu\text{m}$  at low temperatures ( $\sim 550 \text{ }^\circ\text{C}$ ) and strain rates of  $10^{-5}$  to  $10^{-3} \text{ s}^{-1}$  is superplastic with an  $m$  value of  $\sim 0.48$  and total elongation up to 1000%. Superplastic deformation of the ultrafine Ti–6Al–4V under the optimal conditions does not give rise to noticeable cavitation.
2. Ultrafine Ti–6Al–4V undergoes measurable static coarsening of  $\alpha$  over periods of time of the order of 0–100 h. This coarsening follows  $t^3$  vs time kinetics and is thus diffusion controlled.
3. Dynamic coarsening at low temperatures (550 °C) occurs at rates which are approximately two orders of magnitude faster than the corresponding static-coarsening rates. This behavior can be ascribed to the enhancement of diffusion through the deformed  $\beta$  matrix.
4. The very high mechanical properties, limited cavitation, and the large difference in static vs dynamic microstructural coarsening of the ultrafine alloy at 550 °C can be associated with the redistribution of the  $\beta$  phase from triple-junction locations to the matrix during SP deformation.

## Acknowledgments

The main part of this work was supported by the Russian Ministry of Education and Science via Project No. 11.1816.2014/K at Belgorod State University. The results on wetting of  $\alpha/\alpha$  boundaries (B.B. Straumal) was supported by the Russian Foundation for Basic Research (grants 16-53-12007 and 15-53-06008), the Deutsche Forschungsgemeinschaft, and the Russian Federal Ministry for Education and Science (Increase Competitiveness Program of NUST«MISIS»K1-2015-026). The authors are also grateful to the personnel of the Joint Research Centre, Belgorod State University, for their assistance with the experimental analysis.

## References

- [1] O.A. Kaibyshev, *Superplasticity of Alloys, Intermetallics, and Ceramics*, Springer-Verlag, Berlin, 1992.
- [2] T.G. Nieh, J. Wadsworth, O.D. Sherby, *Superplasticity in Metals and Ceramics*, Cambridge University Press, Cambridge, 1997.
- [3] R.Y. Lutfullin, A.A. Kruglov, R.V. Safullin, M.K. Mukhametrakhimov,

- O.A. Rudenko, Processing properties of nano- and submicro-crystalline Ti-6Al-4V titanium alloy, *Mater. Sci. Eng. A* 503 (2009) 52–54.
- [4] J.E. Bird, A.K. Mukherjee, J.E. Dorn, Experimental Correlations between high-temperature creep behavior and structure, in: D.G. Brandon, A. Rosen (Eds.), *Quantitative Relation Between Microstructure and Properties*, Israel Universities Press, Jerusalem, Israel, 1969, pp. 255–342.
  - [5] S.L. Semiatin, P.N. Fagin, J.F. Betten, A.P. Zane, A.K. Ghosh, G.A. Sargent, Plastic flow and microstructure evolution during low-temperature superplasticity of ultrafine Ti-6Al-4V sheet material, *Metall. Mater. Trans. A* 41A (2010) 499–512.
  - [6] Y.G. Ko, C.S. Lee, D.H. Shin, S.L. Semiatin, Low-temperature superplasticity of ultra-fine-grained Ti-6Al-4V processed by equal-channel angular pressing, *Metall. Mater. Trans. A* 37A (2006) 381–391.
  - [7] A.V. Sergueeva, V.V. Stolyarov, R.Z. Valiev, A.K. Mukherjee, Superplastic behavior of ultrafine-grained Ti-6Al-4V alloy, *Mater. Sci. Eng. A* 323 (2002) 318–325.
  - [8] G.A. Salishchev, E.A. Kudryavtsev, S.V. Zharebtsov, S.L. Semiatin, Low temperature superplasticity of Ti-6Al-4V processed by warm multidirectional forging, *Mater. Sci. Forum* 735 (2013) 253–258.
  - [9] H. Matsumoto, K. Yoshida, S.-H. Lee, Y. Ono, A. Chiba, Ti-6Al-4V alloy with an ultrafine-grained microstructure exhibiting low-temperature-high-strain-rate superplasticity, *Mater. Lett.* 98 (2013) 209–212.
  - [10] G.A. Salishchev, O.R. Valiakmetov, V.A. Valitov, S.K. Mukhtarov, Submicrocrystalline and nanocrystalline structure formation in materials and search for outstanding superplastic properties, *Mater. Sci. Forum* 170–172 (1994) 121–130.
  - [11] Y. Mishin, C. Herzig, Diffusion in the Ti-Al system, *Acta Mater.* 48 (2000) 589–623.
  - [12] S.V. Zharebtsov, G.A. Salishchev, R.M. Galeev, O.R. Valiakmetov, S.Yu. Mironov, S.L. Semiatin, Production of submicrocrystalline structure in large-scale Ti-6Al-4V billet by warm severe deformation processing, *Scr. Mater.* 51 (2004) 1147–1151.
  - [13] S. Zharebtsov, E. Kudryavtsev, S. Kostjuchenko, S. Malysheva, G. Salishchev, Strength and ductility-related properties of ultrafine grained two-phase titanium alloy produced by warm multiaxial forging, *Mater. Sci. Eng. A* 536 (2012) 190–196.
  - [14] G. Salishchev, O. Valiakmetov, W. Beck, F.H. Froes, Production of Ti-6Al-4V sheets for low temperature superplastic forming, *Mater. Sci. Forum* 551–552 (2007) 31–36.
  - [15] ASM Handbook. *Mechanical Testing and Evaluation*, vol. 8. Materials Park, OH: ASM International; 2000.
  - [16] G.A. Sargent, A.P. Zane, P.N. Fagin, A.K. Ghosh, S.L. Semiatin, Low-temperature coarsening and plastic flow behavior of an alpha/beta titanium billet material with an ultrafine microstructure, *Metall. Mater. Trans. A* 39A (2008) 2949–2964.
  - [17] S. Zharebtsov, M. Murzinova, G. Salishchev, S.L. Semiatin, Spheroidization of the lamellar microstructure in Ti-6Al-4V alloy during warm deformation and annealing, *Acta Mater.* 59 (2011) 4138–4150.
  - [18] H. Sharma, S.M.C. van Bohemen, R.H. Petrov, J. Sietsma, Three-dimensional analysis of microstructures in titanium, *Acta Mater.* 58 (2010) 2399–2407.
  - [19] Y.-T. Wang, Y. Adachi, K. Nakajima, Y. Sugimoto, Quantitative three-dimensional characterization of pearlite spheroidization, *Acta Mater.* 58 (2010) 4849–4858.
  - [20] J.W. Martin, R.D. Doherty, B. Cantor, *Stability of Microstructure in Metallic Systems*, Cambridge University Press, Cambridge, 1997.
  - [21] S.L. Semiatin, B.C. Kirby, G.A. Salishchev, Coarsening behavior of an alpha-beta titanium alloy, *Metall. Mater. Trans. A* 35A (2004) 2809–2819.
  - [22] S. Zharebtsov, G. Salishchev, S.L. Semiatin, Loss of coherency of the alpha/beta interface boundary in titanium alloys during deformation, *Philos. Mag. Lett.* 90 (2010) 903–914.
  - [23] S.L. Semiatin, S.L. Knisley, P.N. Fagin, F. Zhang, D.R. Barker, Microstructure evolution during alpha-beta heat treatment of Ti-6Al-4V, *Metall. Mater. Trans. A* 34A (2003) 2377–2386.
  - [24] A. Ball, M.M. Hutchinson, Superplasticity in the aluminum-zinc eutectoid, *Met. Sci. J.* 3 (1969) 1–6.
  - [25] A.K. Mukherjee, The rate controlling mechanism in superplasticity, *Mater. Sci. Eng.* 8 (1971) 83–89.
  - [26] T.G. Langdon, Grain boundary sliding as a deformation mechanism during creep, *Philos. Mag.* 22 (178) (1970) 689–700.
  - [27] R.C. Gifkins, Grain-boundary sliding and its accommodation during creep and superplasticity, *Metall. Trans. A* 7A (1976) 1225–1232.
  - [28] H. Ogi, S. Kai, H. Ledbetter, R. Tarumi, M. Hirao, K. Takashima, Titanium's high-temperature elastic constants through the hcp–bcc phase transformation, *Acta Mater.* 52 (2004) 2075–2080.
  - [29] S.L. Semiatin, G.A. Sargent, Constitutive modeling of low-temperature superplastic flow of ultrafine Ti-6Al-4V sheet material, *Key Eng. Mater.* 433 (2010) 235–240.
  - [30] S.L. Semiatin, T.M. Brown, T.A. Goff, P.N. Fagin, D.R. Barker, R.E. Turner, J.M. Murry, J.D. Miller, F. Zhang, Diffusion coefficients for modeling the heat treatment of Ti-6Al-4V, *Metall. Mater. Trans. A* 35A (2004) 3015–3018.
  - [31] J.F. Murdock, T.S. Lundy, E.E. Standsbury, Diffusion of  $Ti^{44}$  and  $V^{48}$  in titanium, *Acta Metall.* 12 (1964) 1033–1039.
  - [32] N.E. Walsøe De Reca, C.M. Libanati, Autodifusión de titanio beta y hafnio beta, *Acta Metall.* 16 (1968) 1297–1305.
  - [33] J.F. Murdock, C.J. McHargue, Self-diffusion in body-centered cubic titanium-vanadium alloys, *Acta Metall.* 16 (1968) 493–500.
  - [34] G.A. Lopez, E.J. Mittemeijer, B.B. Straumal, Grain boundary wetting by a solid phase; microstructural development in a Zn–5 wt% Al alloy, *Acta Mater.* 52 (2004) 4537–4545.
  - [35] M. Takashima, P. Wynblatt, B.L. Adams, Correlation of grain boundary character with wetting behavior, *Interface Sci.* 8 (2000) 351–361.
  - [36] S. Curiotto, D. Chatain, Solid/liquid interfacial energy and wetting of Cu at Co surfaces and grain boundaries, *Scr. Mater.* 60 (2009) 40–43.
  - [37] B.B. Straumal, A.S. Gornakova, Y.O. Kucheev, B. Baretzky, A.N. Nekrasov, Grain boundary wetting by a second solid phase in the Zr-Nb alloys, *J. Mater. Eng. Perform.* 21 (2012) 721–724.
  - [38] A.S. Gornakova, S.I. Prokofiev, K.I. Kolesnikova, B.B. Straumal, Formation regularities of grain-boundary interlayers of the  $\alpha$ -Ti phase in binary titanium alloys, *Russ. J. Non-Ferrous Met.* 57 (2016) 229–235.
  - [39] A.S. Gornakova, S.I. Prokofiev, B.B. Straumal, K.I. Kolesnikova, Growth of ( $\alpha$ )Ti grain boundary layers in Ti-Co alloys, *Russ. J. Non-Ferrous Met.* 56 (2016) 437–441.
  - [40] B.B. Straumal, X. Sauvage, B. Baretzky, A.A. Mazilkin, R.Z. Valiev, Grain boundary films in AlZn alloys after high pressure torsion, *Scr. Mater.* 70 (2014) 59–62.
  - [41] B.B. Straumal, A. Korneva, O. Kogtenkova, L. Kurmanaeva, P. Zięba, A. Wierzbicka-Miernik, S.N. Zhevnenko, B. Baretzky, Grain boundary wetting and premelting in the Cu-Co alloys, *J. Alloys Compd.* 615 (S1) (2014) S183–S187.
  - [42] M.I. Mazurski, G.A. Salishchev, Effect of interface anisotropy on the thermal stability and transformation of lamellar structures: I. Behavior of two-phase systems under annealing as related to particle shape equilibrium, *Phys. Stat. Sol. (b)* 187 (1995) 501–509.
  - [43] M.I. Mazurski, G.A. Salishchev, Effect of interface anisotropy on the thermal stability and transformation of lamellar structures: II. Transformation of lamellae, *Phys. Stat. Sol. (b)* 188 (1995) 653–658.
  - [44] J.M. Howe, H.I. Aaronson, J.P. Hirth, Aspects of interphase boundary structure in diffusional phase transformations, *Acta Mater.* 48 (2000) 3977–3984.
  - [45] T. Furuhara, H.J. Lee, E.S.K. Menon, H.I. Aaronson, Interphase boundary structures associated with diffusional phase transformations in Ti-base alloys, *Metall. Mater. Trans. A* 21A (1990) 1627–1643.
  - [46] M.L. Meier, D.R. Lesuer, A.K. Mukherjee,  $\alpha$  grain size and  $\beta$  volume fraction aspects of the superplasticity of Ti-6Al-4V, *Mater. Sci. Eng. A* 136 (1991) 71–78.
  - [47] M.L. Meier, D.R. Lesuer, A.K. Mukherjee, The effects of the  $\alpha/\beta$  phase proportion on the superplasticity of Ti-6Al-4V and iron-modified Ti6Al4E4V, *Mater. Sci. Eng. A* 154 (1992) 165–173.
  - [48] X. Jiang, J. Cui, L. Ma, A cavity nucleation model during high temperature creep deformation of metals, *Acta Metall. Mater.* 41 (1993) 539–542.
  - [49] A.H. Chokshi, Cavity nucleation and growth in superplasticity, *Mater. Sci. Eng. A* 410–411 (2005) 95–99.
  - [50] R. Raj, Nucleation of cavities at second phase particles in grain boundaries, *Acta Metall.* 26 (1978) 995–1006.
  - [51] H. Reidel, *Fracture at High Temperatures*, Springer-Verlag, Berlin, 1987.